J Solid State Electrochem (2004) 8: 599–605
DOI 10.1007/s10008-003-0488-3

ORIGINAL PAPER

H. J. M. Bouwmeester · M. W. Den Otter
B. A. Boukamp

Oxygen transport in $La_{0.6}Sr_{0.4}Co_{1-y}Fe_yO_{3-\delta}$

Received: 25 May 2003 / Accepted: 29 September 2003 / Published online: 23 March 2004

Abstract The surface exchange coefficient and chemical diffusion coefficient of oxygen for the perovskites $La_{0.6}Sr_{0.4}Co_{1-y}Fe_yO_{3-\delta}$ ($y = 0.2$, 0.5 and 0.8) were measured using the conductivity relaxation technique. Measurements were performed between 600 and 800 °C in an oxygen partial pressure range between 10^{-4} and 1 bar. Both transport coefficients decrease markedly with decreasing oxygen partial pressure below about 10^{-2} bar at all temperatures. This is attributed to ordering of oxygen vacancies. Implications for using $La_{0.6}Sr_{0.4}Co_{1-y}Fe_yO_{3-\delta}$ as an oxygen separation membrane are discussed.

Keywords Chemical diffusion · Conductivity relaxation · Mixed ionic-electronic conductors · Perovskites · Surface exchange

Introduction

Mixed conducting perovskites, $La_{0.6}Sr_{0.4}Co_{1-y}Fe_yO_{3-\delta}$, have attracted interest due to their possible use as ceramic membranes for the separation of oxygen from air [1]. Another potential application involves use as a cathode for low-temperature solid oxide fuel cells [2]. The substitution of divalent strontium for trivalent lanthanum in the parent compound $LaCoO_{3-\delta}$ causes the formation of oxygen vacancies, enhancing the ionic conductivity. The co-substitution of iron for cobalt improves its chemical stability, albeit at the expense of ionic conductivity. The ionic conductivity in the series at temperatures 700-1000 °C, however, remains 1-2 orders of magnitude higher than that found for stabilized zirconia [3]. The presence of multivalent cations ensures a high, predominantly electronic, conductivity.

Besides high diffusivities of oxygen, the applications require fast rates for the surface oxygen exchange reaction. In a previous study on $La_{1-x}Sr_xCoO_{3-\delta}$ perovskites, we found that both the surface exchange coefficient and chemical diffusivity of oxygen decrease profoundly upon lowering the oxygen partial pressure below about 10^{-2} bar at temperatures of 600-850 °C [4]. These observations were attributed to vacancy ordering at reduced oxygen partial pressures. In this paper, the conductivity relaxation technique is employed for the study of oxygen transport in perovskite compositions $La_{0.6}Sr_{0.4}Co_{1-y}Fe_yO_{3-\delta}$.

Presented at the OSSEP Workshop "Ionic and Mixed Conductors: Methods and Processes", Aveiro, Portugal, 10-12 April 2003

H. J. M. Bouwmeester (✉) · M. W. Den Otter · B. A. Boukamp
Department of Science & Technology,
MESA Institute for Nanotechnology, University of Twente,
P.O. Box 217, 7500 AE Enschede, The Netherlands
E-mail: h.j.m.bouwmeester@ct.utwente.nl

Theory

The conductivity relaxation technique involves measurement of the time variation of the electrical conductivity of a sample after a stepwise change in the ambient oxygen partial pressure. The sample responds to this change by an uptake or release of oxygen, i.e. changing its oxygen content, and, through that, its electrical conductivity. Both the surface reaction rate and chemical diffusion in the bulk may impose a limitation on the overall oxygen transport. The relaxation data are fitted to theoretical equations using the surface exchange coefficient K_{tr} and the chemical diffusion coefficient $\tilde{D}$ as fitting parameters.

In the analysis of the diffusion problem, a flat thin sheet is considered with thickness $2b$. At $t < 0$, the sample is assumed to be in thermodynamic equilibrium with the surrounding atmosphere. At $t = 0$, the p_{O_2} is changed stepwise to a new value, corresponding with a new equilibrium oxygen concentration, c_∞. Depending on the value of c_∞ relative to c_0, the oxygen concentration at $t < 0$, oxygen starts to diffuse into or out of the sample.

The starting point in the derivation is Fick's second law:

$$\frac{\partial c}{\partial t} = \tilde{D}\frac{\partial^2 c}{\partial z^2} \tag{1}$$

where $\tilde{D}$ is the chemical diffusion coefficient. The surface reaction is assumed to proceed at a rate proportional to the difference between the actual concentration at the surface, $c(\pm b)$, and c_∞. The boundary conditions at surfaces $z = b$ and $z = -b$ are then given by:

$$J(b) = -\tilde{D}\frac{\partial c}{\partial z}\bigg|_{z=b} = K_{\mathrm{tr}}[c(b) - c_\infty] \tag{2}$$

and:

$$J(-b) = -\tilde{D}\frac{\partial c}{\partial z}\bigg|_{z=-b} = -K_{\mathrm{tr}}[c(-b) - c_\infty] \tag{3}$$

respectively, where J denotes the flux density. The solution for the concentration profile as a function of time, $c(z,t)$, is obtained through an eigenfunction expansion of the initial oxygen concentration c_0 [5]:

$$\frac{c(z,t) - c_0}{c_\infty - c_0} = 1 - \sum_{n=1}^{\infty} \frac{2L_\beta \cos(\beta_n z/b)}{\left(\beta_n^2 + L_\beta^2 + L_\beta\right)\cos(\beta_n)} \exp\left(-\frac{t}{\tau_n}\right) \tag{4}$$

where the time constants τ_n are given by:

$$\tau_n = \frac{b^2}{\tilde{D}\beta_n^2} \tag{5}$$

and the parameters β_n are obtained from:

$$\beta_n \tan \beta_n = \frac{bK_{\mathrm{tr}}}{\tilde{D}} = L_\beta \tag{6}$$

Equating the change in oxygen nonstoichiometry to changes in electrical conductivity, it is possible to express the dimensionless conductivity transient $\sigma(t)$ as:

$$\bar{\sigma}(t) = \frac{\sigma(t) - \sigma_0}{\sigma_\infty - \sigma_0} = 1 - \sum_{n=1}^{\infty} \frac{2L_\beta^2}{\beta_n^2\left(\beta_n^2 + L_\beta^2 + L_\beta\right)} \exp\left(-\frac{t}{\tau_n}\right) \tag{7}$$

Equation (7) is based on a linearized relation between conductivity and oxygen concentration. Provided that the step change in oxygen partial pressure is small, this is generally a reasonable assumption. Using this equation it is possible to obtain the parameters $\tilde{D}$ and K_{tr} from the experimental relaxation data provided that $0.03 < L_\beta < 30$. As outlined previously by den Otter et al. [6], $\tilde{D}$ cannot be obtained from the relaxation data if $L_\beta < 0.03$. In that case the equilibration kinetics towards the new oxygen nonstoichiometry is entirely governed by the rate of the surface reactions. On the other hand, if $L_\beta > 30$, the transient is not affected by the surface reactions and only $\tilde{D}$ can be derived from the fitting procedure. A simple numerical method for the evaluation of the eigenvalues β_n has been presented elsewhere [7].

Experimental

Preparation

Powders of composition $La_{0.6}Sr_{0.4}Co_{1-y}O_{3-\delta}$ with $y = 0.2$, 0.5 and 0.8 were prepared by thermal decomposition of precursor complexes derived from nitrate solutions using ethylenediaminetetraacetic acid (EDTA) as a complexing agent [8]. The pH of the nitrate solution containing stoichiometric amounts of the constituent metals was adjusted to a value of 9 by adding NH_4OH. The mixture was then condensed and heated until pyrolysis occurred. The product was calcined at 925 °C in stagnant air for 10 h to remove remaining carbon. X-ray powder diffraction confirmed formation of a single-phase perovskite in all cases. After calcination, the powders were milled and isostatically pressed at 4000 bar followed by sintering at 1200 °C in air for 10 h. Heating and cooling rates were 0.3 °C min^{-1}. For conductivity relaxation experiments, thin rectangular samples were cut from the sintered bodies, which showed relative densities in excess of 95%. The samples were polished with 1000 mesh SiC to 0.53 mm×15 mm×25 mm dimensions and ultrasonically cleaned in ethanol prior to use.

Thermogravimetry

The oxygen nonstoichiometry as a function of temperature and p_{O_2} was calculated from corresponding thermogravimetry data (Setaram Setsys 16). A powder sample of about 1000 mg was annealed in situ in nitrogen-diluted oxygen ($p_{O_2} = 0.9$ bar) at 900 °C for 3 h. The sample was subsequently cooled down to room temperature at 2 °C min^{-1}.

Using mass flow controllers (Brooks 5850) for nitrogen and oxygen, the p_{O_2} was adjusted to values in the range 0.01-0.9 bar. Measurements were carried out at 500, 600, 700, 800 and 900 °C, both upon heating from room temperature to 900 °C and subsequent cooling to room temperature. At each of these temperatures the sample was allowed to equilibrate for 1-3 h. Heating and cooling rates were 2 °C min^{-1}. No significant hysteresis was observed. The oxygen nonstoichiometry was calculated from the weight change, assuming that the sample at a p_{O_2} of 0.9 bar exhibits ideal oxygen stoichiometry at room temperature, as was found to hold for the compositions $La_{0.6}Sr_{0.4}Co_{1-y}Fe_yO_{3-\delta}$ ($y = 0.0$, 0.1,0.25, 0.4, 0.6) in air [9].

Conductivity relaxation

The samples were mounted in a small-volume quartz reactor chamber (20 cm^3) and subsequently pre-annealed at 900 °C for 3 h in oxygen. The actual experiments were performed over the p_{O_2} range from 10^{-4} to 1 bar at temperatures between 600 and 800 °C. Figure 1 shows a schematic diagram of the measurement set-up.

Step changes in p_{O_2} were achieved by switching between two separate nitrogen-diluted oxygen gas flows at 300 mL min^{-1} (STP) using an electrical four-way valve. For oxidizing (reducing) runs, the p_{O_2} of the vented flow was set three times higher (lower) than that of the gas flow through the reactor. The estimated flushtime of the reactor was less than 0.75 s at 700 °C. Gas flows with p_{O_2} values below 0.2% were obtained using a home-made YSZ-based oxygen pump. A commercial oxygen sensor (SYSTECH ZR893/4) was used for the p_{O_2} measurement.

Relative changes in the sample's electrical conductivity following a step change in p_{O_2} were measured by an a.c. four-probe technique using gold wire electrodes. Measurements were performed using a lock-in amplifier (EG&G Princeton Applied Research 5210, Ireland), which was operated at a frequency (1259 Hz) high enough to probe fast decay processes. Resistance changes as low as 2% could be resolved. Conductivity transients were analysed

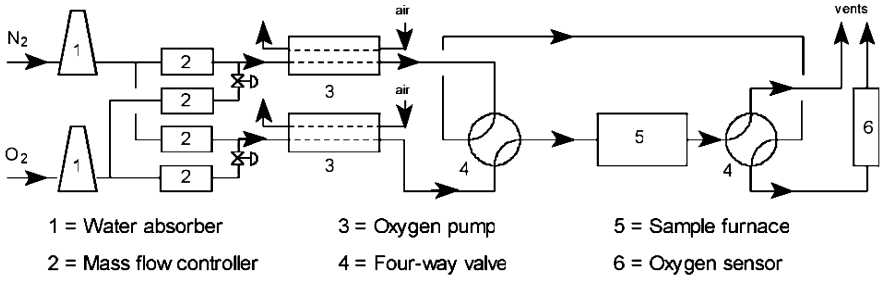

Fig. 1 Scheme of the oxygen conductivity relaxation set-up

using self-developed curve-fitting software that utilizes the Levenberg-Marquardt method to perform nonlinear regression (the software is available at http://ims.tnw.utwente.nl).

Results and discussion

Oxygen nonstoichiometry

Data for oxygen nonstoichiometry of $La_{0.6}Sr_{0.4}Co_{1-y}Fe_yO_{3-\delta}$ ($y=0.2$, 0.5 and 0.8) as obtained from thermogravimetric measurements are given in Fig. 2. It can be seen that the parameter δ for each of the compositions varies almost linearly with the logarithm of p_{O_2}. The results are consistent with previous data from our laboratory [9], showing that the linear relationship holds at least over the p_{O_2} range 10^{-5}-1 bar, and with those obtained by others [10, 11]. However, the results contradict those found in [12].

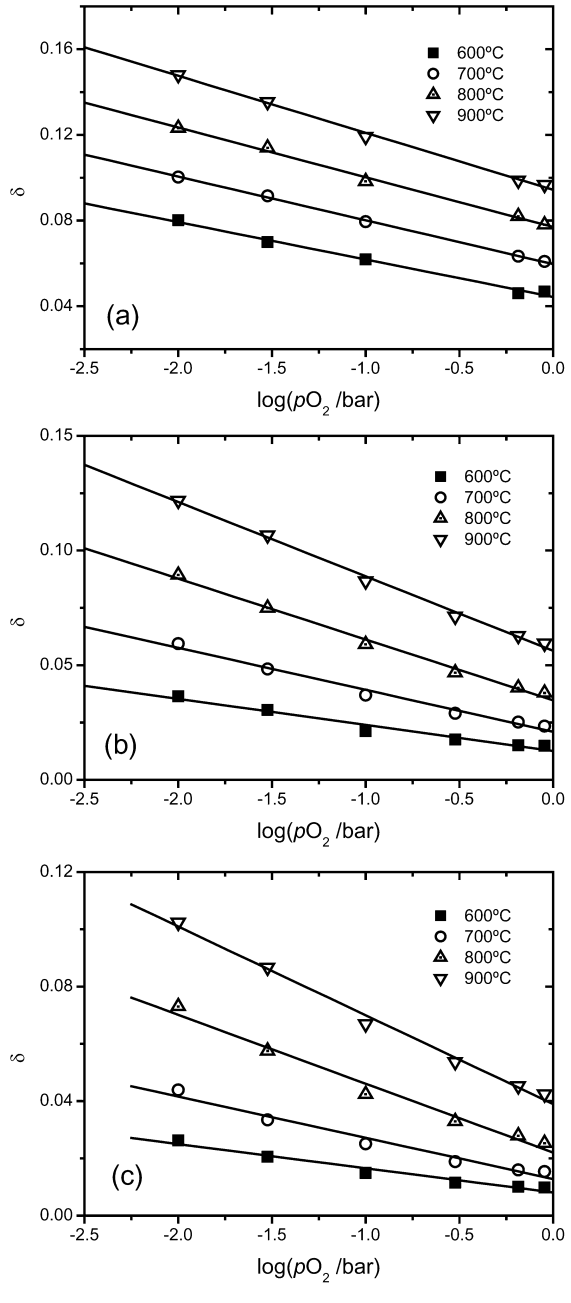

Fig. 2 Oxygen nonstoichiometry of $La_{0.6}Sr_{0.4}Co_{1-y}Fe_yO_{3-\delta}$ plotted as a function of oxygen partial pressure at different temperatures: (**a**) $y=0.2$, (**b**) $y=0.5$ and (**c**) $y=0.8$

Electrical conductivity

Figure 3 shows the dependence of the total electrical conductivity on oxygen partial pressure for $La_{0.6}Sr_{0.4}Co_{1-y}Fe_yO_{3-\delta}$ ($y=0.2$, 0.5 and 0.8) at different temperatures. The results obtained are found to be consistent with those obtained by others. The observed behaviour is typical for that of the acceptor-doped perovskite oxides in which charge compensation occurs both by ionic and electronic defects.

Using the Kröger-Vink notation, the dissolution of SrO in the La(Fe,Co)O_3 perovskite lattice can be described by:

$$2SrO + 2La_{La}^{\times} + \frac{1}{2}O_2 + 2Fe_{Fe}^{\times} \xrightarrow{La(Fe,Co)O_3} La_2O_3 + 2Sr'_{La} + 2Fe_{Fe}^{\bullet} \quad (8)$$

where it is assumed that electronic charge compensation occurs, preferentially by a valence change of the iron ions over cobalt ions, or:

$$2SrO + 2La_{La}^{\times} + O_O^{\times} \xrightarrow{La(Fe,Co)O_3} La_2O_3 + 2Sr'_{La} + V_O^{\bullet\bullet} \quad (9)$$

in which reaction charge compensation occurs by the formation of doubly ionized oxygen vacancies. The extent of oxygen nonstoichiometry is further determined by the equilibrium reaction of oxygen from the lattice with that from the gas phase:

$$\begin{cases} 2Fe_{Fe}^{\bullet} + O_O^{\times} \rightleftharpoons \frac{1}{2}O_2 + V_O^{\bullet\bullet} + 2Fe_{Fe}^{\times} \\ 2Co_{Fe}^{\bullet} + O_O^{\times} \rightleftharpoons \frac{1}{2}O_2 + V_O^{\bullet\bullet} + 2Co_{Fe}^{\times} \end{cases} \quad (10)$$

Since the ionic and electronic compensations occur simultaneously and compete with each other, the charge neutrality condition, assuming only localized electronic charge carriers to be present, can be expressed as:

$$2\left[V_O^{\bullet\bullet}\right] + \left[Fe_{Co}^{\bullet}\right] + \left[Co_{Co}^{\bullet}\right] = \left[Sr'_{La}\right] \quad (11)$$

where the presence of n-type charge carriers has been omitted. Their contribution to the electrical conductivity may occur at a low enough oxygen partial pressure as a result of charge disproportionation reactions: $2Fe^{3+} \rightleftharpoons Fe^{2+} + Fe^{4+}$ and $2Co^{3+} \rightleftharpoons Co^{2+} + Co^{4+}$. For each fully ionized vacancy formed in the lattice, two p-type charge carriers are eliminated. Accordingly, the decrease of the electrical conductivity with oxygen partial pressure inferred from Fig. 3 can be explained by the reduction of the concentration of p-type charge

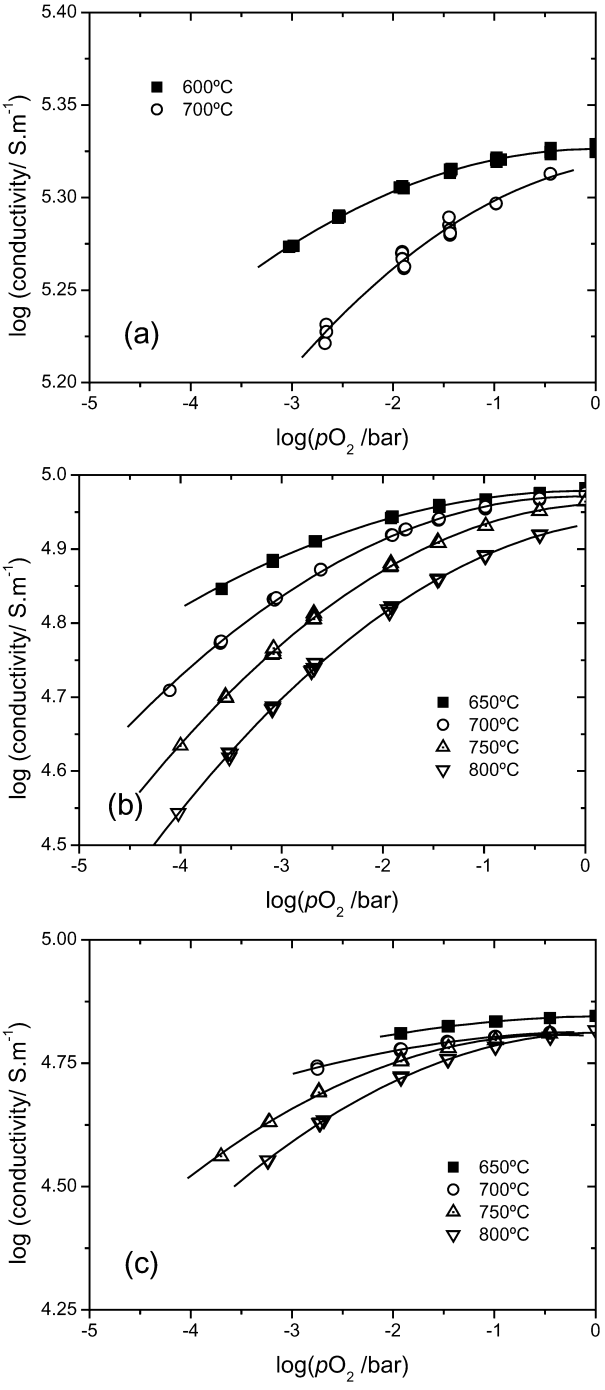

Fig. 3 Total conductivity of $La_{0.6}Sr_{0.4}Co_{1-y}Fe_yO_{3-\delta}$ plotted as a function of oxygen partial pressure at different temperatures: (**a**) $y=0.2$, (**b**) $y=0.5$ and (**c**) $y=0.8$

carriers, associated with the tetravalent states of the cobalt and iron atoms, as oxygen vacancies are formed. The decrease is less profound in those regions of the oxygen partial pressure, where electronic compensation is the preferred mechanism of charge compensation. Owing to the greater mobility of the electronic defects over that of the ionic defects, it can safely be assumed that the data shown in Fig. 3 refer to the electronic conductivity only.

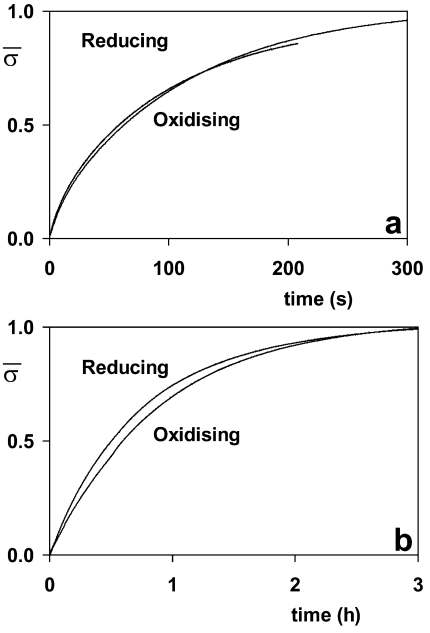

Fig. 4 Normalized conductivity data for $La_{0.6}Sr_{0.4}Co_{1-y}Fe_yO_{3-\delta}$ at 750 °C following oxidation and reduction step changes to the same final oxygen partial pressure: (**a**) $\dot{p}_{O_2}=0.35$ bar and (**b**) $p_{O_2}=0.28\times10^{-3}$ bar

Electrical conductivity in $La_{1-x}Sr_xCo_{1-y}Fe_yO_{3-\delta}$ compositions in the usual ranges of temperature and oxygen partial pressure has been interpreted by two-site hopping of p-type small polarons [13] and by a mixed model [9]. In the latter, adiabatic hopping of small polarons (through Fe^{3+} and Fe^{4+} sites) occurs simultaneously with a more band-like conduction via states of mixed Co 3d-O 2p character. It is seen from Fig. 3 that the conductivity of $La_{1-x}Sr_xCo_{1-y}Fe_yO_{3-\delta}$ at a given oxygen partial pressure and temperature decreases with increasing Fe content. This behaviour is attributed to reflect not only the enhanced carrier concentration if iron is substituted for cobalt, but also the more conductive nature of the cobalt sites relative to the iron sites.

Conductivity relaxation

Figure 4 shows typical conductivity relaxation transients for $La_{0.6}Sr_{0.4}Co_{0.5}Fe_{0.5}O_{3-\delta}$ at two different oxygen partial pressures. Similar results were obtained in this study for other compositions and temperatures. In both Fig. 4a and Fig. 4b the results for oxidation and reduction step changes to the same final p_{O_2} are shown. It can be seen that good matching is obtained in the case when the final p_{O_2} is equal to 0.35 bar. At the lower value of 0.28×10^{-3} bar (Fig. 4b) the experimental data are affected by the flow rate of the gas. The oxygen released by the sample upon a reduction step change is quickly flushed away by the imposed gas stream. However, given a finite flow rate of the gas stream, the oxygen taken up

by the sample cannot be supplied at a rate high enough upon an oxidation step change when its p_{O_2} is too low. In general, mass transfer limitations during oxidation runs were encountered at p_{O_2} values below about 0.03 bar. Since the ideal step change is better approximated in a reduction experiment, only data derived from these experiments are presented throughout this paper.

Figures 5 and 6 show, respectively, the chemical diffusion coefficient, $\tilde{D}$, and surface exchange coefficient, K_{tr}, as a function of p_{O_2} for $La_{0.6}Sr_{0.4}Co_{1-y}Fe_yO_{3-\delta}$ ($y = 0.2$, 0.5 and 0.8) at different temperatures for each of the compositions. As the p_{O_2} is reduced the value of K_{tr} decreases, while $\tilde{D}$ remains fairly constant. Both parameters decrease profoundly with decreasing p_{O_2} below about 10^{-2} bar. Katsuki et al. [10], using a thermogrametric technique, observed a similar trend in their data for $La_{0.6}Sr_{0.4}Co_{0.8}Fe_{0.2}O_{3-\delta}$. A similar p_{O_2} dependence of $\tilde{D}$ and K_{tr} was also found in our previous study on oxygen transport in $La_{1-x}Sr_xCoO_{3-\delta}$ ($x = 0.2$, 0.5 and 0.7) [4]. The results are further consistent with relaxation data presented for $La_{0.6}Sr_{0.4}Co_{0.2}Fe_{0.8}O_{3-\delta}$ [14, 15].

To be able to judge the merit of the above results, the transport of oxygen in the defective perovskite structure has to be considered. Such a transport is generally considered to occur via a vacancy diffusion mechanism. In accord with the Wagner theory, $\tilde{D}$ can be expressed as:

$$J(b) = -\tilde{D}\frac{\partial c}{\partial x}\bigg|_{x=b} = K_{tr}[c(b) - c_\infty] \tag{12}$$

where F is the Faraday constant, σ_{ion} and σ_{el} are the partial ionic and electronic conductivities, c_O is the concentration of oxygen in the perovskite, and μ_{O_2} the oxygen chemical potential. The derivative in Eq. (12), $\frac{\partial \mu_{O_2}}{\partial c_O}$, termed the thermodynamic factor, can be evaluated directly from data for oxygen nonstoichiometry as a function of oxygen partial pressure, according to:

$$\frac{\partial \mu_{O_2}}{\partial c_O} = -V_m \frac{\partial \mu_{O_2}}{\partial \delta} = -V_m \frac{\partial \ln p_{O_2}}{\partial \delta} \tag{13}$$

where V_m is the perovskite molar volume. Owing to the prevailing electronic conductivity of the perovskites $La_{0.6}Sr_{0.4}Co_{1-y}Fe_yO_{3-\delta}$ in ranges of temperature and p_{O_2} of interest, Eq. 13 can thus be rewritten as:

$$\tilde{D} \approx -\frac{RTV_m}{8F^2}\sigma_{ion}\frac{\partial \ln p_{O_2}}{\partial \delta} \tag{14}$$

Owing to the linear relationship found between δ and $\log(p_{O_2})$ for $La_{0.6}Sr_{0.4}Co_{1-y}Fe_yO_{3-\delta}$, as shown in Fig. 2, the thermodynamic factor for each of the compositions at all temperatures becomes constant. The corollary is that changes in $\tilde{D}$ and σ_{ion} follow the same trend upon varying p_{O_2}. The magnitude of the ionic conductivity in oxygen-deficient perovskites is closely tied to the thermal disordering of oxygen vacancies, the degree of which may depend both on temperature and oxygen partial pressure. A tentative explanation for the above observations is therefore that at reduced p_{O_2} values not all lattice oxygens are involved in transport due to vacancy ordering. Adler et al. [16] have provided evidence, using high-temperature oxygen-17 NMR, that in the related perovskites $La_{0.6}Sr_{0.4}Co_{0.8}Cu_{0.2}O_{3-\delta}$ and $La_{0.5}Ba_{0.5}Co_{0.7}Cu_{0.3}O_{3-\delta}$ below approximately 800 °C only a few oxygen vacancies are mobile, while the remainder is

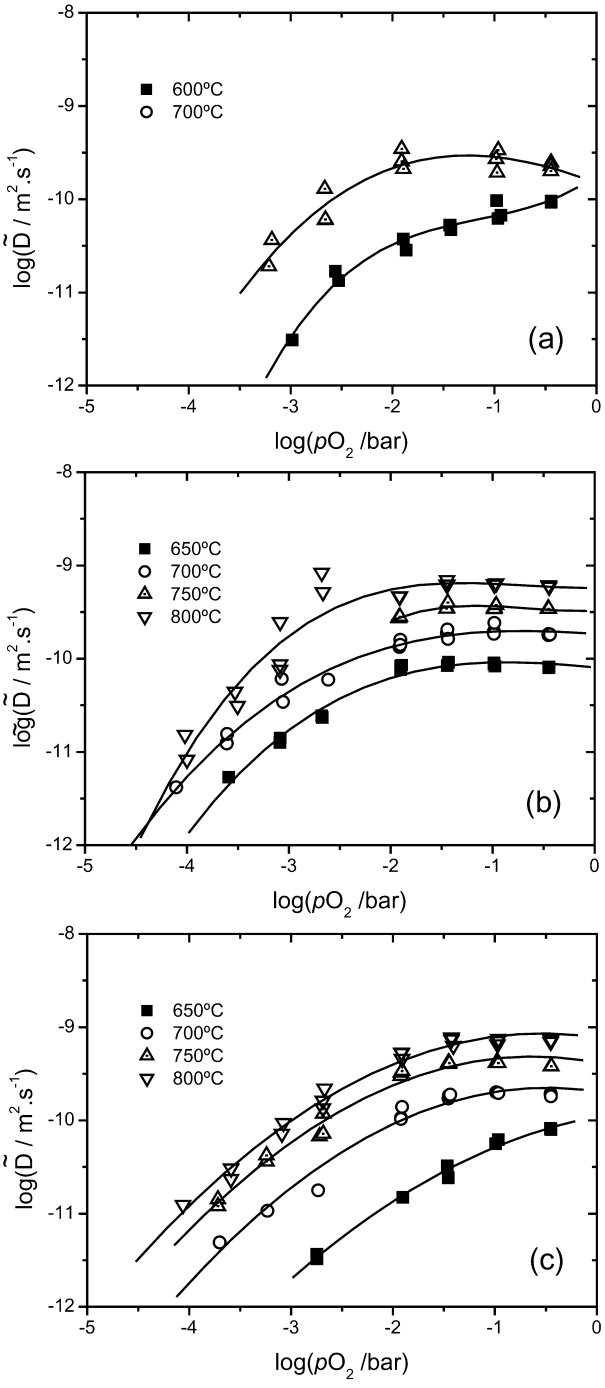

Fig. 5 Chemical diffusion coefficient of $La_{0.6}Sr_{0.4}Co_{1-y}Fe_yO_{3-\delta}$ plotted as a function of oxygen partial pressure at different temperatures: (**a**) $y = 0.2$, (**b**) $y = 0.5$ and (**c**) $y = 0.8$

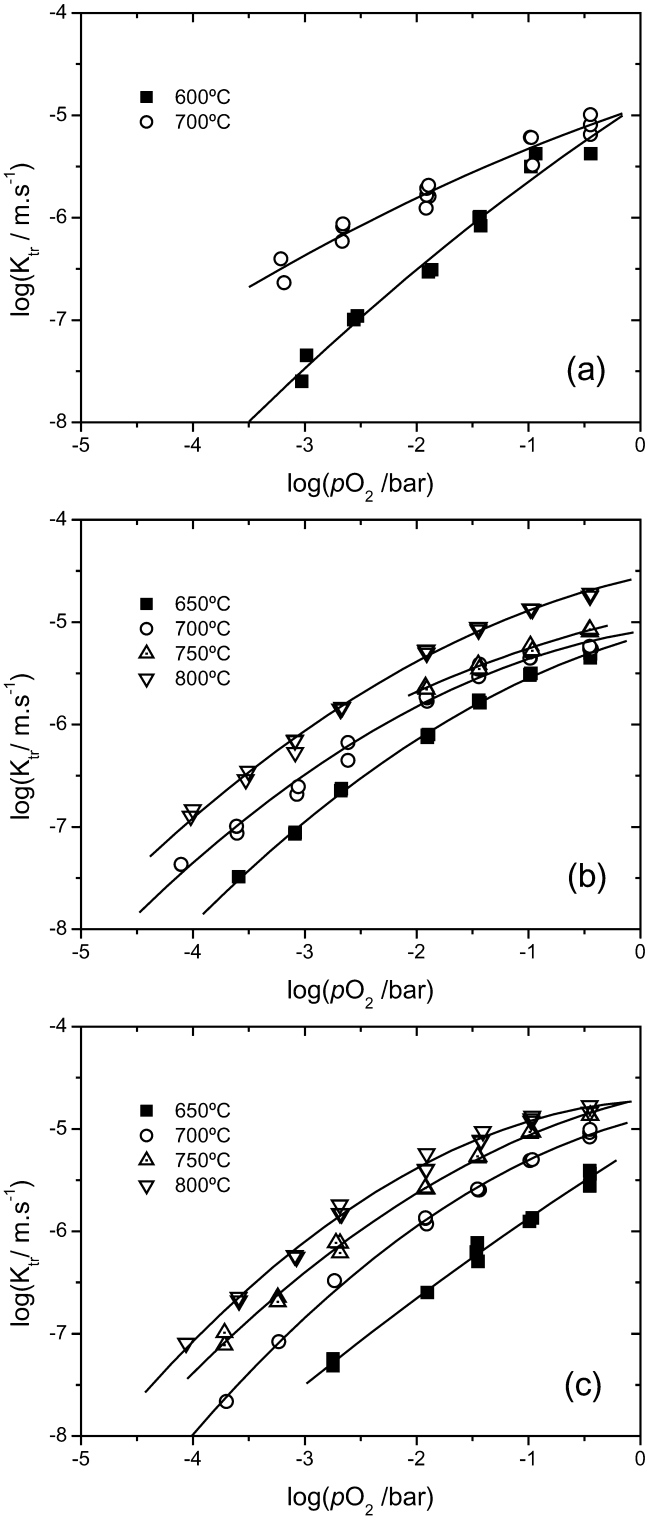

Fig. 6 Surface exchange coefficient of $La_{0.6}Sr_{0.4}Co_{1-y}Fe_yO_{3-\delta}$ plotted as a function of oxygen partial pressure at different temperatures: (**a**) $y = 0.2$, (**b**) $y = 0.5$ and (**c**) $y = 0.8$

trapped in ordered layers, accommodated in domains on a length scale 50-500 Å. Above 800 °C, the signal intensity was found to increase steadily with temperature, up to the maximum temperature of 950 °C in their experiments, suggesting a concomitant increase in the number of mobile oxygen vacancies.

Table 1 Apparent activation energies of the transport parameters for $La_{0.6}Sr_{0.4}Co_{1-y}Fe_yO_{3-\delta}$. Values are given in kJ mol^{-1}

	$y = 0.2$	$y = 0.5$	$y = 0.8$	p_{O_2} (10^{-3} bar)
$\tilde{D}$	113	122	180	12
$\tilde{D}$	-	118	180	0.36
K_{tr}	129	122	214	12
K_{tr}	82	115	181	0.36

The fact that $\tilde{D}$ and K_{tr} both decrease with decreasing p_{O_2} suggests a correlation between these parameters. The correlation is reinforced by the observation that both parameters exhibit almost similar activation energies, as listed in Table 1, and implies that the concentration of oxygen vacancies plays a prime role in determining the rate of both processes.

Conclusions

The profound decline in oxygen chemical diffusivity and associated ionic conductivity observed for the phases $La_{0.6}Sr_{0.4}Co_{1-y}Fe_yO_{3-\delta}$ in the range 600-800 °C below a p_{O_2} of approximately 10^{-2} bar is tentatively attributed to the ordering of oxygen vacancies. It is believed to be induced by the increased vacancy concentration and the enhanced interactions between them at low oxygen partial pressures. An important corollary from this result is that it affects the profile of the oxygen chemical potential under real operating conditions of mixed-conducting membranes by contrast with a material in which oxygen vacancies are randomly distributed, all contributing to the ionic conductivity. If $La_{0.6}Sr_{0.4}Co_{1-y}Fe_yO_{3-\delta}$ were to be employed as a ceramic membrane in a reactor for methane conversion processes, the oxygen chemical potential profile is predicted to be very steep at the low p_{O_2} side of the membrane. This not only leads to differential expansion at this side of the membrane, due to the concomitant change in the concentration of oxygen vacancies, but also to steep gradients in the chemical potentials of the cations which arise as a consequence of the Gibbs-Duhem relation. This leads to kinetic demixing/decomposition phenomena if the diffusivities of the involved cations are non-negligible and eventually will cause mechanical failure.

Our mechanistic understanding of the oxygen surface exchange reaction is fairly rudimentary. Surface reconstruction, impurity segregation and other surface phenomena can all have a significant impact on the exchange rate. Kilner et al. [17] noted that the surface exchange coefficient and self diffusivity are actually related for a range of mixed-conducting perovskites. Assuming that the surface vacancy is the site at which surface exchange takes place, the authors derived an expression for the surface exchange rate in terms of bulk atomistic parameters. In our recent study on the perovskites $La_{1-x}Sr_xCoO_{3-\delta}$, we found a near linear rela-

tionship between the surface exchange coefficient and the chemical diffusivity which even holds in those regions of temperature and p_{O_2} where vacancy ordering occurs [4]. This observation suggests that the surface oxygen exchange coefficient is directly proportional to the mobile fraction of oxygen vacancies. It is to be expected that vacancy-ordered structures or regions at or near the (sub-)surface effectively block the surface exchange reaction. The apparent correlation between both parameters for the phases $La_{0.6}Sr_{0.4}Co_{1-y}Fe_yO_{3-\delta}$ found in this study can be interpreted similarly and adds to the existing body of evidence that it is the oxygen vacancy and its nature that play a crucial role in determining the magnitude of the surface exchange rate.

References

1. Bouwmeester HJM, Burggraaf AJ (1997) Dense ceramic membranes for oxygen separation. In: Gellings PJ, Bouwmeester HJM (eds) CRC handbook of solid state electrochemistry. CRC, Boca Raton, chap 14
2. Steele BCH (2000) Solid State Ionics 134:3
3. Teraoka Y, Zhang HM, Okamoto K, Yamazoe N (1988) Mater Res Bull 23:51
4. Van de Haar LM, den Otter MW, Morskate M, Bouwmeester HJM, Verweij H (2002) J Electrochem Soc 149:J41
5. Crank J (1979) The mathematics of diffusion, 2nd edn. Oxford University Press, Oxford, p 60
6. Den Otter MW, Bouwmeester HJM, Boukamp BA, Verweij H (2001) J Electrochem Soc 148:J1
7. Den Otter MW, Van der Haar LM, Bouwmeester HJM (2000) Solid State Ionics 134:259
8. Van Doorn RHE, Kruidhof H, Nijmeijer A, Winnubst L, Burggraaf AJ (1998) J Mater Chem 8:2109
9. Lankhorst MHR, Ten Elshof JE (1997) J Solid State Chem 130:302
10. Katsuki M, Wang S, Dokya M, Hashimoto T (2003) Solid State Ionics 156:453
11. Mantzavinos D, Hartley A, Metcalfe IS, Sahibzada M (2000) Solid State Ionics 134:103
12. Lane JA, Benson SJ, Waller D, Kilner JA (1999) Solid State Ionics 121:201
13. Tai L-W, Nasrallah MM, Anderson HU, Sparlin DM, Sehlin SR (1995) Solid State Ionics 76:273
14. Sahibzada M, Morton W, Hartley A, Mantzavinos D, Metcalfe IS (2000) Solid State Ionics 136/137:991
15. Lane JA, Kilner JA (2000) Solid State Ionics 136/137:997
16. Adler S, Russek S, Reimer J, Fendorf M, Stacy A, Huang Q, Santoro A, Lynn J, Baltisberger J, Werner U (1994) Solid State Ionics 68:193
17. Kilner JA, De Souza RA, Fullarton IC (1996) Solid State Ionics 86/88:703